Defect-mediated hydrogen-bond melting in *B*-DNA polymers

V. V. Prabhu, L. Young, K. W. Awati, W. Zhuang, and E. W. Prohofsky
Department of Physics, Purdue University, West Lafayette, Indiana 47907
(Received 28 August 1989)

This paper explores the melting temperatures of the hydrogen bonds that hold together the two strands of DNA. We choose as samples both homopolymers and copolymers of DNA. First, we investigate the melting temperatures of hydrogen bonds throughout the polymer via a mean-field approach. Then a defect is introduced by cutting the hydrogen bonds in one unit cell at room temperature. We study the propagation of this defect to neighboring cells with rise in temperature. The calculation is a modified self-consistent phonon approach. The agreement between the calculated melting temperatures and observed melting temperatures is excellent for defected melting. The defected melting is an approximation to initiation-site melting.

I. INTRODUCTION

Hydrogen bonds between complementary bases, along with nonbonded interactions, hold the two strands of the deoxyribonucleic acid (DNA) helix together. The base paris could be adenine-thymine (A-T) or guanine-cystosine (G-C). The melting of these hydrogen bonds is a prerequisite for biologically significant transcription or replication.

We study this melting of hydrogen bonds in two stages. First, we explore how these bonds weaken and collapse as the temperature rises; this we accomplish by a modified mean-field self-consistent phonon approach (MSPA).[1,2] While the MSPA provides melting temperatures, it forces corresponding bonds in every unit cell of the polymer to weaken simultaneously. A better simulation of the actual process of melting is to introduce a defect in one unit cell by setting some or all hydrogen-bond force constants to zero at room temperature. Introducing a defect is the second stage of our study. We then examine the reduction in the force constants of the hydrogen bonds in the neighboring cells with the rise in temperature, thus enabling the propagation of this defect.[3]

The introduction of this defect is an attempt to mimic actual melting, as it is known from critical-exponent analysis that melting usually arises from an initiation site. The initiation site arises from fluctuations not treated in mean-field theories. A second reason for introducing a defect is to have a crude approximation to the type of melting that is needed in elongation of the open state in biological processes. The melting of cells adjacent to the defect is taken as the better melting temperature, since it indicates the onset of growth of the initiation site.

Force constants of hydrogen bonds weaken with increases in their stretch amplitudes. With rise in temperature, the stretch amplitudes increase, thereby reducing the force constants. This enhances the stretches even more, and we find ourselves iterating in a self-consistent loop of stretch amplitudes and force constants. The temperature at which there is breakdown of this self-consistency, as reflected in a sudden divergence in stretch amplitudes or sudden reduction in force constants, is taken as the melting temperature of the hydrogen bonds.

Kim *et al.*[2,3] have explored melting in poly(dG)·poly(dC). Here, we first study the homopolymer poly(dA)·poly(dT). Sufficiently sharp ir modes are experimentally observable[4] in this homopolymer, and melting experiments can be meaningfully related to those observations. Then we explore poly(dA-dG)·poly(dC-dT) in great detail as an example of a more complicated system. In two sections hereafter, we describe setting up the self-consistent loop and its breakdown, first, for the MSPA and then for defect-mediating melting. The defect in poly(dA)·poly(dT) consists of cutting all hydrogen bonds in cell 0. For the copolymer poly(dA-dG)·poly(dC-dT), this study is extended over three kinds of defects. First, only the A-T bonds in cell 0 are cut, keeping the G-C bonds intact. Then the hydrogen bonds of G-C in cell 0 are cut, keeping the A-T bonds intact. Finally, we create a defect in which the hydrogen bonds of both A-T and G-C are cut in cell 0. We compare these results with those of poly(dA-dC)·poly(dG-dT).[5] In this paper we refer to the polymer poly(dA)·poly(dT) as A-T, poly(dG)·poly(dC) as G-C, poly(dA-dG)·poly(dC-dT) as AGCT, and poly(dA-dC)·poly(dG-dT) as ACGT.

II. THE LOOP IN THE MSPA

In our model all force constants in the DNA lattice except for those of the hydrogen bonds are restricted to their fitted harmonic potentials. The hydrogen bonds are treated as asymmetric Morse potential wells, V, where

$$V = V_0\{1-\exp[-a(R-R_0)]\}^2 - V_0 \ . \tag{1}$$

Here, R is the length of the hydrogen bond, and a, V_0, and R_0 are constant. (See Table I.) The Morse constants are determined for A-T and G-C and assumed the same for ACGT and AGCT. The effective force constant ϕ_i of the ith hydrogen bond, weighted over stretches s_i in the well, is

TABLE I. Hydrogen-bond constants.

Base pair	Bond	$R_{293\ K}$ (Å)	k (mdyn/Å)	V_0 (mdyn Å)	a (1/Å)	R_0 (Å)
A-T	N(1) · · · H—N(3)	2.9002	0.115	0.0168	2.517	2.761
A-T	N(6)—H · · · O(4)	2.8801	0.116	0.0193	2.732	2.694
G-C	N(1)—H · · · N(3)	2.8694	0.157	0.0183	2.349	2.805
G-C	O(6) · · · H—N(4)	2.8065	0.243	0.0256	2.875	2.694
G-C	N(2)—H · · · O(2)	2.8092	0.235	0.0250	2.781	2.705

$$\phi_i = \frac{\int ds_i\, e^{-s_i^2/2D_i} \dfrac{d^2V}{ds_i^2}}{\int ds_i\, e^{-s_i^2/2D_i}} \ . \tag{2}$$

This effective force constant is initially set equal to the harmonic force constant found from the Lippincott-Schroeder model.[6] Here, D_i is the weighted mean-square stretch amplitude of the ith hydrogen bond:

$$D_i = \langle s_i s_i \rangle \ , \tag{3}$$

$$D_i = \frac{1}{\pi} \sum_j \int_0^{\pi} d\theta \frac{1}{2\omega_j(\theta)} \{\coth[\beta\omega_j(\theta)/2]\} s_i^j(\theta) s_i^{j*}(\theta) \ , \tag{4}$$

where $s_i^j(\theta)$ is the component of the eigenvector of the ith hydrogen-bond stretch of band j at angle θ. j and θ refer to the dispersion curve of the lattice, j being the band of eigenfrequencies ω_j and θ being the equivalent of the momentum in the first Brillouin zone.

The eigenvalues and eigenfrequencies of the lattice at room temperature are found from the secular equation[1]

$$[\mathbf{F} - \omega^2 \mathbf{I}]\xi(\theta) = 0 \ , \tag{5}$$

where $\mathbf{F}$ is the matrix of force constants in internal coordinates. This matrix includes nonbonded force constants and implicitly includes hydrophobic interactions that help hold the DNA helix together. The force constants are determined as the second derivative of the potential energy at the energy minimum. The minima are determined by the inclusion of all hydrophobic interactions. The force constants are fitted to experimental observations.[7–9] The nonbonded interactions are of the form

$$f_{ij} = \left| \frac{2\eta e_i e_j}{\sqrt{\epsilon_i}\sqrt{\epsilon_j} r_{ij}^3} - \frac{42A}{r_{ij}^8} + BC^2 e^{-Cr_{ij}} \right| \ , \tag{6}$$

where f_{ij} is the force constant (in units of mdyn/Å) of the nonbonded stretch coordinate and r_{ij} the distance in angstroms between atoms i and j. Here atoms i and j are in adjacent base pairs. The coordinates are from Arnott *et al.*[10] We have chosen charges from Miller.[11] The nonbonded interactions emerging from these charges were fitted by us to experimentally observed neutron-scattering data,[9] forming the basis of our choice of dielectric constants. This fitting has since worked consistently well for all copolymers in reproducing melting temperatures.

ϵ_i is the charge on atom i, $\eta = 2.31$, $A = 1.85$, $B = 209.2$, and $C = 3.7$. ϵ_i is the dielectric constant associated with atom i. A unit cell of a copolymer has two base pairs in it, while the comparing unit cell of the homopolymer has only one base pair. Hence the dielectric constant associated with atom i is taken as 1.0 inside the unit cell of a copolymer, and this value of the dielectric constant is raised to its long-range value outside the unit cell. For homopolymers, this value is taken to vary linearly with distance.[12] Also, for homopolymers, f_{ij} has a slightly different form:

$$f_{ij} = \left| \frac{2\eta e_i e_j}{\sqrt{\epsilon_i}\sqrt{\epsilon_j} r_{ij}^3} - \frac{42A}{r_{ij}^8} \right| \ , \tag{7}$$

where $\eta = 2.31$, and A has been adjusted to a value of 0.12 to fit far-infrared-absorption data for a homopolymer.[12] These two slightly different forms of f_{ij} are found to be essential to reproduce spectroscopic data from the dispersion curves. The slight variations in the form of f_{ij} for homopolymers and copolymers arises from the fact that we have used the standard form of nonbonded interactions from the literature[13] for copolymers. In the case of homopolymers, however, better experimental data are available, which enables a more precise fitting.

Having incorporated the appropriate force constants in $\mathbf{F}$, the diagonalization in Eq. (5) yields the eigenfrequencies and eigenvectors at room temperature.

When the temperature is raised, the new eigenvectors and eigenfrequencies are calculated as follows. If $C_i^m = \bar{\phi}_i - \phi_i$ is the change in the force constant of the ith hydrogen bond, then Eq. (5) is modified to

$$[\mathbf{F} - \omega^2 \mathbf{I} + \mathbf{C}^m]\xi(\theta) = 0 \ . \tag{8}$$

The superscript m on C^m refers to mean-field melting. Instead of solving this equation to get new eigenfrequencies and eigenvectors, we use a Green's function $\mathbf{g}(\omega^2, \theta)$ as

$$\mathbf{g}(\omega^2, \theta) = [\omega^2 \mathbf{I} - \mathbf{F}(\theta)]^{-1} \ . \tag{9}$$

Then Eq. (8) reduces to

$$[\mathbf{I} - \mathbf{g}(\omega^2, \theta) C^m]\xi(\theta) = 0 \ . \tag{10}$$

Hence, the new eigenfrequencies are determined by

$$|\mathbf{I} - \mathbf{g}\mathbf{C}^m| = 0 \ . \tag{11}$$

However, $\mathbf{C}^m$ is of dimension n, where n is the number of hydrogen bonds in a unit cell. Thus, $\mathbf{I} - \mathbf{g}\mathbf{C}^m$ is of very small order. The new eigenvectors $\bar{s}_i^{\lambda}(\theta)$ are determined by a simple perturbation approximation:

TABLE II. Melting temperatures (in K).

Polymer	Mean field	Defect, A-T cut in cell 0	Defect, G-C cut in cell 0	Defect, all bonds cut in cell 0	Expt.
A-T	350	310			326
G-C[a]	380		350		360
ACGT	385	355	350	350	350
AGCT	355	345	345	350	343

[a]References 2 and 3.

$$\bar{s}_i^{\alpha}=s_i^{\alpha}+\sum_{\lambda\neq\alpha}\sum_{j}\frac{s_j^{\lambda *}C_j^m s_j^{\alpha}}{\omega_{\alpha}^2-\omega_{\lambda}^2}s_i^{\lambda}\ . \tag{12}$$

Using the new frequencies in Eq. (11), we recalculate the force constant $\bar{\phi}_i$ in Eq. (2) and calculate the difference in $C_i^m=\bar{\phi}_i-\phi_i$. This is the difference in the values of the force constant of each hydrogen bond between the present and previous iterations. If this difference consistently decreases for successive iterations at a given temperature, then C_i^m is convergent. If, after a few iterations, C_i^m increases for any hydrogen bond, its behavior is divergent.

Starting from 300 K, we perform iterations and examine convergence in intervals of 5 or 10 K. We iterate at each temperature tested until

$$\Delta=\frac{\prod_{i=1}^{n}C_i^m}{\prod_{i=1}^{n}\phi_i}<(0.01)^n\ . \tag{13}$$

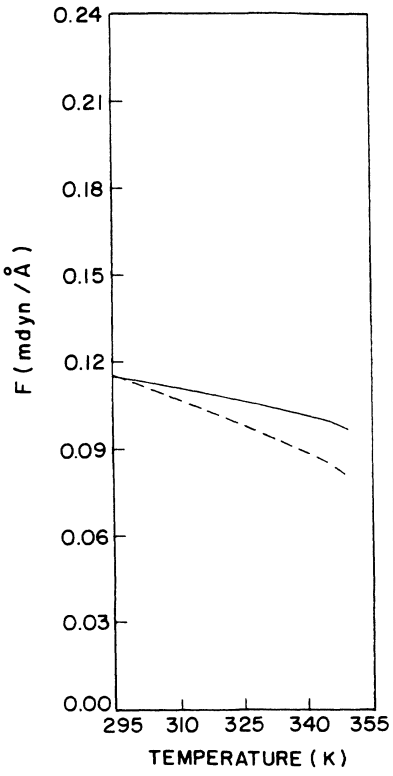

FIG. 1. Mean-field melting of hydrogen bonds in A-T. The lines refer to the same bonds as in Fig. 2.

We watch for the instability $\Delta/\Delta_0>1.0$, where Δ_0 is from the previous iteration. The temperature at which this instability manifests itself is taken as the melting temperature of the hydrogen bonds. We note that this is the temperature at which the instability sets in for all unit cells of the polymer simultaneously. Column 2 in Table II lists the mean-field melting temperatures of all four polymers.

The choice of the position coordinates used, the values of the Morse-potential parameters and the form of the long-range nonbonded interactions are most important. Arnott *et al.* have two versions of *B*-DNA polymer coordinates obtained in different refinements, which we shall refer to here as refinements 1 (Ref. 10) and 2 (Ref. 14). The two refinements, differing in the explicit treatment of the hydrogen atoms, yield base pairs whose hydrogen-

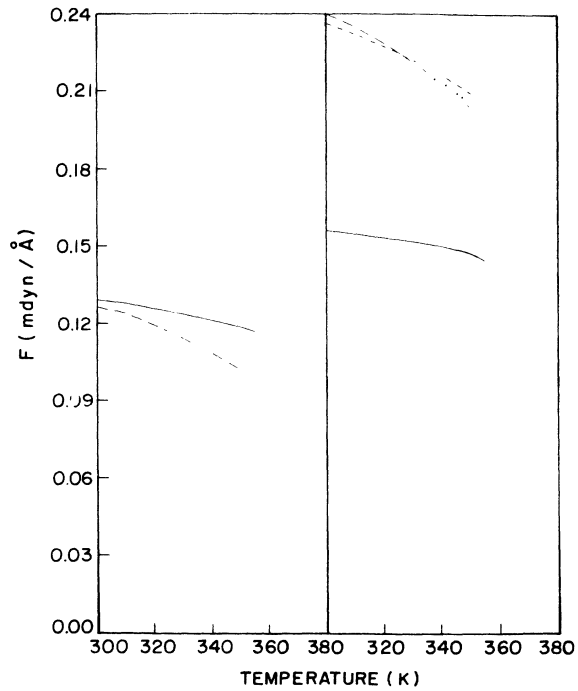

FIG. 2. Mean-field melting of hydrogen bonds in AGCT. The two bonds to the left are of the base pair A-T, while the three bonds to the right are of the base pair G-C. The solid line is the N(1)—H · · · N(3) bond on both sides. The long-dashed line is the N(6)—H · · · O(4) bond on the A-T side and O(6) · · · H—N(4) on the G-C side. The short-dashed line on the G-C side is the N(2)—H · · · O(2) bond. The first and second halves of the temperature axis denote the same range of temperature.

bond lengths are different. Coordinates drawn from refinement 2 create rather long hydrogen bonds. Since we use the Lippincott-Schroeder[6] model to calculate hydrogen-bond force constants, our calculated force constants are inversely proportional to the lengths of the hydrogen bonds. The strength of these force constants affect the melting temperature. Earlier we had performed mean-field melting calculations with coordinates from refinement 2.[1] Those coordinates created hydrogen bonds with very weak force constants in A-T (0.053 as compared to 0.116 in refinement 1). Subsequent calculations revealed that these coordinates created anomalies wherever hydrogen bonds were specifically relevant. It was therefore found essential to explore melting in coordinates drawn from refinement 1.

The previous paper also had the disadvantage of only the 13 lowest bands being accurately treated, the remaining 233 bands of the dispersion curve having been considered in the Einstein approximation. It was subsequently found that frequencies around 90 cm^{-1} (bands 25–30) contributed substantially to hydrogen-bond stretches. Here, 27 bands are treated exactly.

The crucial difference, however, is in the choice of the Morse-potential parameters and here a significant point is

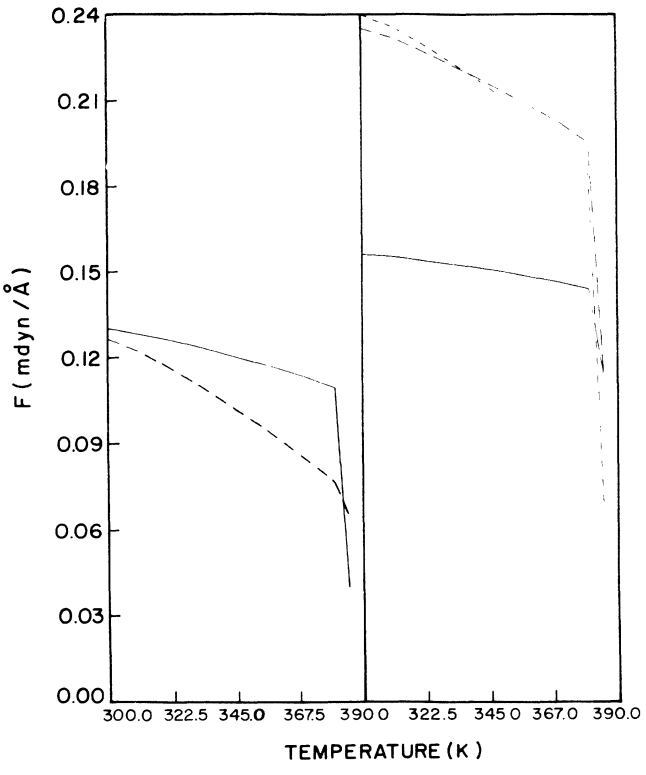

FIG. 3. Mean-field melting of hydrogen bonds in ACGT. The two bonds to the left are of the base pair A-T, while the three bonds to the right are of the base pair C-G. The solid line is the N(1)···H—N(3) bond on both sides. The long-dashed line is the N(6)—H···O(4) bond on the A-T side and N(2)—H···O(2) on the C-G side. The short-dashed line on the C-G side is the O(6)···H—N(4) bond. The first and second halves of the temperature axis denote the same range of temperature.

to be made. There are two principal methods of choosing the Morse-potential parameters. The first rests on the constancy of force constants and the second on the constancy of potentials of corresponding hydrogen bonds in homopolymers and copolymers.

The first method, followed in the previous paper, assumes that the harmonic force constants of hydrogen bonds in the homopolymers A-T and G-C will also be the harmonic force constants of A-T and G-C bonds in the copolymers. Then the Morse parameters have to be recalculated for each copolymer to ensure this constancy of force constants. The melting temperatures calculated for the copolymers through such a procedure reproduce the correct order only when the form of the long-range nonbonded force constants are altered so as to suit each polymer.

The second method, followed in this paper, is to ensure that the potentials of A-T and G-C bonds are retained for corresponding bonds in the copolymers. For AGCT and ACGT they reproduce the correct order in melting temperatures with no parameters adjusted and no variation in the long-range force-constant model. We calculate a mean-field melting temperature of 355 K for AGCT and, upon inverting G-C to C-G, creating ACGT, the mean-field temperature is raised to 385 K. Figures 1, 2, and 3 display the mean-field melting of hydrogen bonds in AT, AGCT, and ACGT, respectively.

III. THE SELF-CONSISTENT LOOP IN DEFECT-MEDIATED MELTING

Here we set to zero the force constants of some or all hydrogen bonds in a given unit cell called cell 0. We specifically examine the change in force constants of the remaining hydrogen bonds, if any, in cell 0, and of the hydrogen bonds in the adjoining cells, called cell $+1$ and cell -1. The temperature at which there is a breakdown in the force constants of cells ± 1 is taken as the melting temperature, as it indicates the onset of growth of the initiation site.[3]

When hydrogen bonds are cut in cell 0, in addition to in-band normal modes of the lattice there now arise localized modes. If D_i^N is the mean-square stretch amplitude from the in-band modes and D_i^L that from the localized modes, D_i for hydrogen bonds in either cell $+1$, 0, or -1 is

$$D_i = D_i^N + D_i^L \ . \tag{14}$$

D_i^N is calculated as follows. In cutting hydrogen bonds in cell 0, the force constants of hydrogen bonds in cells $+1$ and -1 are perturbed. If C is the diagonal Green-function source matrix, where C_i is the change in force constants of hydrogen bonds in cell $+1$, 0, or -1, the secular equation [Eq. (5)] is modified to

$$|\mathbf{F}-\omega^2\mathbf{I}+\mathbf{C}|=0 \ . \tag{15}$$

If $\mathbf{G}$ is $[\omega^2\mathbf{I}-\mathbf{F}-\mathbf{C}]^{-1}$, then

$$D_i^N = \frac{1}{\pi}\overline{\int} d\omega \coth\left[\beta\frac{\omega}{2}\right] \mathrm{Im}G_i(\omega^2) \ , \tag{16}$$

where $\overline{\int}$ indicates integration over ω for all bands of the perfect helix, and $\mathrm{Im}G_i$ denotes the imaginary part of G_i. **G** can be shown to be

$$\mathbf{G}=(\mathbf{I}-\mathbf{gC})^{-1}\mathbf{g} , \tag{17}$$

where $\mathbf{g}=[\omega^2\mathbf{I}-\mathbf{F}]^{-1}$. Details of the calculation of **g** are found in Kim *et al.*[3] D_i^L, the localized-mode contribution to D_i, is now calculated.

The localized-mode eigenfunctions q_a, for coordinates directly affected by the cut, are given by

$$[1-g_{aa}C_{aa}]q_a=0 , \tag{18}$$

where a refers to coordinates affected by hydrogen bonds severed in cell 0. Eigenfunctions of coordinates not directly affected by the defect are given by

$$q_b=g_{ba}C_{aa}q_a . \tag{19}$$

From the localized-mode eigenfunctions, we can project s_i^λ, which is the localized stretch component of the ith hydrogen bond from the λth band. The localized-mode eigenfunctions are specifically normalized from considerations of energy.[15] The frequencies of the localized modes, ω_λ, are obtained as zeros of the determinant $|1-g_{aa}C_{aa}|$,

$$D_i^L=\sum_L \frac{\coth(\beta\omega_\lambda/2)}{2\omega_\lambda}(s_i^\lambda)(s_i^\lambda)^* . \tag{20}$$

The localized-mode eigenfunctions are calculated at room temperature and assumed to be constant at higher temperatures. Also, the stretch contribution from the modes in the Einstein approximation is directly carried over from the mean-field calculation and assumed to be constant at all temperatures. Having found $D_i=D_i^N+D_i^L$, we recalculate the force constants of hydrogen bonds in cells $+1$, 0, and -1 from Eq. (2). We commence the iteration at each temperature, with D_i calculated from the eigenvectors and eigenfrequencies obtained as consistent solutions of the preceding MSPA calculation at that temperature.

If ϕ_i are the initial force constants of hydrogen bonds at room temperature and $\bar{\phi}_i$ their values after iteration, consider

$$\bar{C}_i=\bar{\phi}_i-\phi_i, \quad i=1,2,\ldots,3n \tag{21}$$

where n is the number of hydrogen bonds in one unit cell. The diagonal matrix $\bar{\mathbf{C}}$, with diagonal elements $\bar{C}_i$, is used in place of C_i in Eqs. (15) and (16), and we iterate in a loop of mean-square stretches and hydrogen-bond force constants of cells $+1$, 0, and -1. At each temperature we iterate until we are assured of convergence in the value of the hydrogen-bond force constants. The temperature at which the force constants reduce distinctly in either cell $+1$ or -1 is considered the melting temperature, for then the instability has begun to grow to the surrounding cells.

IV. RESULTS AND DISCUSSION

Figure 4 shows the defect-mediated hydrogen-bond melting in cells ±1 of A-T when the hydrogen bonds were cut in cell 0. We notice that the instability in cell 0 spreads to both cell $+1$ and cell -1 without any marked preference of direction. For this polymer the mean-field melting temperature was 350 K and the defect-mediated melting temperature was 310 K. The experimentally observed melting temperature is 326 K.

Figure 5 depicts the defect-mediated hydrogen-bond melting in cells 0 and ±1 of AGCT when A-T hydrogen bonds are cut in cell 0. At the top of the figure is cell $+1$; cell 0 is in the middle and cell -1 is at the bottom. The left half of the plot contains the A-T hydrogen bonds and the right half contains the G-C hydrogen bonds. The first and second halves of the temperature axis denote the same range of temperature. We notice that the instability in the G-C bonds demonstrates a mild preference for propagation along the direction cell 0 $\rightarrow$ cell $+1$. This is seen in the fact that the drop in the force constants is sharper in cell $+1$ than in cell -1, at the melting temperature. The drop in cell $+1$ initiates the breakdown of all the hydrogen bonds. This preference is even more distinct in Fig. 6, where the defect in cell 0 comes from cutting the G-C bonds, having retained the A-T bonds intact. The A-T bonds in all three cells, however, collapse due to the large local modes caused by the defect. For both of these cases the defect-mediated melting temperature is 345 K, which compares well with the experimen-

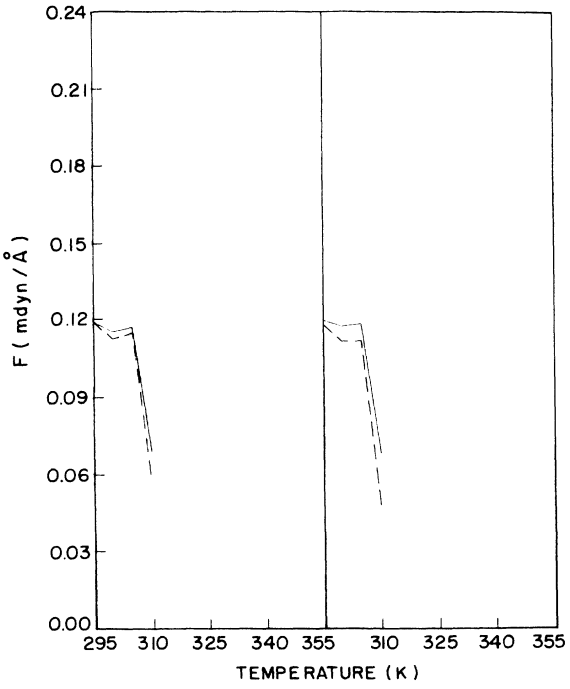

FIG. 4. Hydrogen-bond force constants in cell $+1$ and cell -1 of A-T as a function of temperature when hydrogen bonds in cell 0 are cut. The lines refer to the same bonds as in Fig. 2.

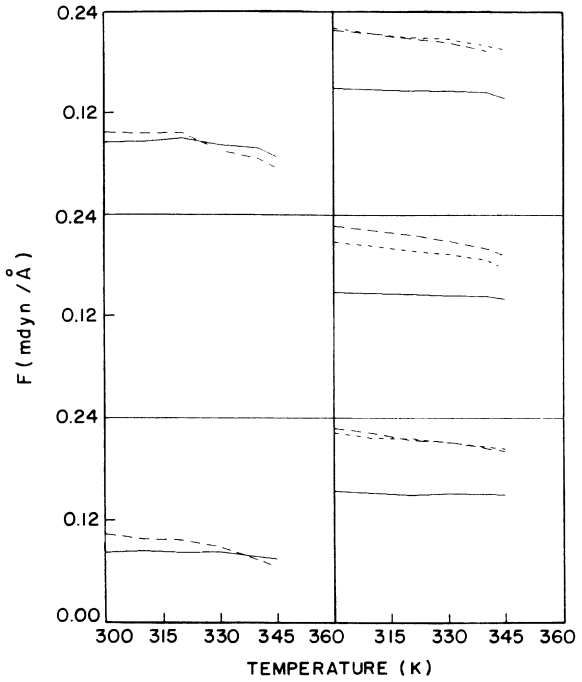

FIG. 5. Force constants in cells 0 and ±1 of AGCT as a function of temperature when A-T hydrogen bonds in cell 0 are cut. The lines refer to the same bonds as in Fig. 2. At the top of the figure is depicted melting of hydrogen bonds in cell +1; in the middle is cell 0 and at the bottom is cell −1. The left of the plot contains A-T bonds in each cell. G-C bonds are in the right half of the plot. The first and second halves of the temperature axis denote the same range of temperature.

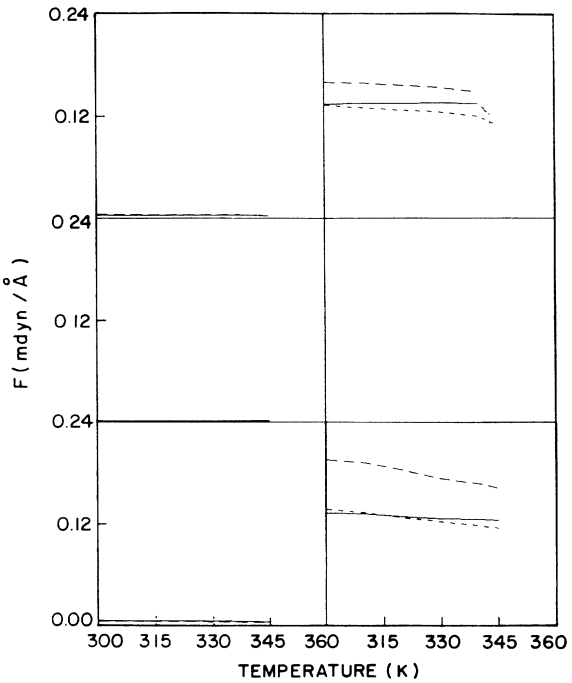

FIG. 6. Variation of hydrogen-bond force constants in cells +1, 0, and −1 of AGCT with temperature when G-C hydrogen bonds are cut in cell 0. The lines refer to the same bonds as in Fig. 2. The instability in cell 0 has a strong preference for propagating in the direction of cell +1.

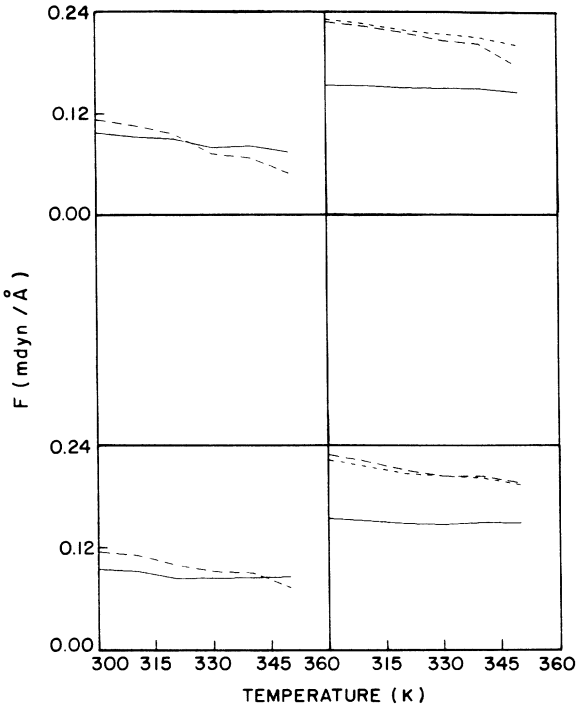

FIG. 7. Variation of hydrogen-bond force constants with temperature in cells +1 and −1 of AGCT when hydrogen bonds of both A-T and G-C are cut in cell 0. The lines refer to the same bonds as in Fig. 2. We track the melting of hydrogen bonds in cells ±1.

tally observed melting temperature of 343 K. The mean-field melting temperature is 355 K.

Figure 7 shows melting of hydrogen bonds in cells ±1 when the hydrogen bonds of both A-T and G-C are severed in cell 0. The melting is not distinct and is at a temperature of 350 K. The initiation site for melting, however, is taken to be a single base pair. Recent calculations of Zhuang *et al.*[16] indicate that the melting temperature does not change for an initiation site up to five base pairs long. The defect-mediated melting plots for all three defects in ACGT have been published elsewhere.[5]

We have summarized, in Table II, the mean-field and defect-mediated melting temperatures of A-T, G-C, AGCT, and ACGT. For both copolymers we have included the melting temperatures for three kinds of defects. Column 3 contains melting temperatures with a defect of A-T hydrogen bonds cut in cell 0, column 4 contains melting temperatures with a defect of G-C bonds cut in cell 0, and column 5 has melting temperatures of the defect with hydrogen bonds of both A-T and G-C cut in cell 0. Column 6 compares these to the experimentally observed melting temperatures,[17] and the agreement is remarkable.

The localization of energy in the hydrogen bonds varies with frequency and temperature. Some frequencies contribute more to the hydrogen-bond stretches than others. The distribution of hydrogen-bond–stretch amplitudes as a function of frequency varies with temperature.

This should be observable as a shift in the frequency of absorption corresponding to the modes with enhanced hydrogen-bond stretches as the temperature increases. The precise prediction of the shifts with temperature would be the next step in these calculations.

ACKNOWLEDGMENTS

This work was supported in part by the U.S. National Institutes of Health under Grant No. GM24443, and by the U.S. Office of Naval Research (ONR) under Grant No. 00014-89-K-0115.

[1]V. V. Prabhu, L. Young, and E. W. Prohofsky, Phys. Rev. B **39**, 5436 (1989).
[2]Y. Kim, K. V. Devi-Prasad, and E. W. Prohofsky, Phys. Rev. B **32**, 5185 (1985).
[3]Y. Kim and E. W. Prohofsky, Phys. Rev. B **33**, 5676 (1986).
[4]J. W. Powell *et al.*, Phys. Rev. A **35**, 3929 (1987).
[5]V. V. Prabhu, L. Young, and E. W. Prohofsky (unpublished).
[6]R. Schroeder and D. Lippincott, J. Phys. Chem. **61**, 921 (1957).
[7]K. C. Lu, E. W. Prohofsky, and L. L. Van Zandt, Biopolymers **16**, 2491 (1977).
[8]K. V. Devi-Prasad and E. W. Prohofsky, Biopolymers **23**, 1795 (1984).
[9]V. V. Prabhu, W. K. Schroll, L. L. Van Zandt, and E. W. Prohofsky, Phys. Rev. Lett. **60**, 1587 (1988).
[10]S. Arnott, P. J. Campbell Smith, and R. Chandrasekaran, in *Handbook of Biochemistry and Molecular Biology,* 3rd ed., edited by G. D. Fasman (Chemical Rubber Co., Cleveland, 1975), Vol. 2, p. 411.
[11]K. J. Miller, Biopolymers **18**, 959 (1979).
[12]L. Young, V. V. Prabhu, and E. W. Prohofksy, Phys. Rev. A **39**, 3173 (1989).
[13]C. M. Venkatachalam and G. N. Ramachandran, *Conformation of Biopolymers* (Academic, New York, 1967).
[14]R. Chandrasekaran and S. Arnott, in *Landolt-Börnstein, Numerical Data and Functional Relationships in Science and Technology,* edited by W. Saenger (Springer-Verlag, Berlin, 1989), Vol. VII/1b.
[15]B. F. Putnam, L. L. Van Zandt, E. W. Prohofsky, and W. N. Mei, Biophys. J. **35**, 271 (1981).
[16]W. Zhuang and E. W. Prohofsky (unpublished).
[17]O. Gotoh and Y. Tagashira, Biopolymers **20**, 1033 (1981).